Large Scale Influences on Summertime Extreme Precipitation in the Northeastern United States

Allison B. Marquardt Collow[1,2], Michael G. Bosilovich[2], and Randal D. Koster[2]

[1]Universities Space Research Association, Columbia, Maryland and Goddard Earth Sciences Technology and Research, Greenbelt, Maryland

[2]Global Modeling and Assimilation Office, NASA Goddard Space Flight Center, Greenbelt, Maryland

Submitted to the *Journal of Hydrometeorology*

Corresponding Author:

Allison B. Marquardt Collow

Global Modeling and Assimilation Office, Code 610.1

NASA Goddard Space Flight Center

Greenbelt, Maryland 20771

Email: allison.collow@nasa.gov

Phone: 301-614-6653

Abstract

Observations indicate that over the last few decades there has been a statistically significant increase in precipitation in the Northeastern United States and that this can be attributed to an increase in precipitation associated with extreme precipitation events. Here we use a state-of-the-art atmospheric reanalysis to examine such events in detail. Daily extreme precipitation events defined at the 75th and 95th percentile from gridded gauge observations are identified for a selected region within the Northeast. Atmospheric variables from the Modern Era Retrospective Analysis for Research and Applications – Version 2 (MERRA-2) are then composited during these events to illustrate the time evolution of associated synoptic structures, with a focus on vertically integrated water vapor fluxes, sea level pressure, and 500 hPa heights. Anomalies of these fields move into the region from the northwest, with stronger anomalies present in the 95th percentile case. Although previous studies show tropical cyclones are responsible for the most intense extreme precipitation events, only 10% of the events in this study are caused by tropical cyclones. On the other hand, extreme events resulting from cut off low pressure systems have increased. The time period of the study was divided in half to determine how the mean composite has changed over time. An arc of lower sea level pressure along the east coast and a change in the vertical profile of equivalent potential temperature suggest a possible increase in the frequency or intensity of synoptic scale baroclinic disturbances.

1. Introduction

Observations indicate that extreme precipitation events have increased throughout the contiguous United States (CONUS), with the largest increase in the northeast region of the country (Janssen et al., 2014; Melillo et al., 2014; Agel et al., 2015; Frei et al., 2015). Flooding associated with extreme precipitation events can result in economic losses and the loss of life, which highlights the need for a complete understanding of such events. An improved understanding of extreme precipitation events and how they will change in the future will help enable the precautions needed to protect society from such events, e.g., through more accurate forecasts.

While it is quite possible that the increasing trend in extreme precipitation events will continue into the future, there is considerable uncertainty (IPCC, 2013; Janssen et al., 2014). The frequency of extreme precipitation events in the Northeast varies by season, and this frequency has changed over time. Significant increases in precipitation in the Northeast have been documented in the fall and on an annual time scale (Kunkel et al., 2013), and a statistically significant increase in extreme precipitation events has been documented during the Northeast warm season (Frei et al., 2015). Many studies have shown that warmer air can hold more water vapor, thereby increasing extreme rainfall; however the increase in extreme precipitation in the Northeast has been shown to exceed that dictated by the Clausius-Clapeyron relationship (Ivancic and Shaw, 2016).

Trends in observed precipitation and extreme precipitation events in the Northeastern United States are further complicated by various meteorological causes that differ in frequency depending on the season and region (Kunkel et al., 2012; Agel et al., 2015; Frei et al., 2015). Extreme precipitation events in the Northeast have been shown to be caused by extratropical

cyclones, tropical cyclones, frontal systems, and mesoscale convective systems (Konrad, 2001; Kunkel et al., 2012; Agel et al., 2015). Tropical cyclones tend to produce the most intense summer and fall extreme precipitation events in the region, whereas frontal systems are the most common cause for an extreme precipitation event during the summer and on an annual time scale (Konrad, 2001; Kunkel et al. 2012); however varying spatial domains and definitions of an extreme precipitation event produce a range of percentages of events caused by tropical cyclones (Barlow, 2011; Kunkel et al., 2012; Agel et al., 2015). Fronts have been shown to be responsible for the vast majority of annual precipitation in major storm track regions and 76% of annual extreme precipitation events in the mid-latitudes (Catto et al., 2012; Catto and Pfahl, 2013).

While previous studies have documented the cause of extreme events in the Northeastern United States, relatively little work has been done to evaluate the climatology of the synoptic structures of these events and how such structures have changed over time in connection with the increase of extreme precipitation. Here we examine these structures in detail, describing the evolution of meteorological fields through the development and aftermath of extreme precipitation events and contrasting, for example, the synoptic structures of weaker and stronger precipitation events to determine what makes an event more extreme. Past studies have suggested there is a weakening of atmospheric circulation during the summer months, prolonging the duration of blocking systems (Coumou et al., 2015). As a result, quasi-stationary patterns could be becoming common and therefore cause an increase in the frequency of extreme precipitation events, which has already been documented in the Balkan Peninsula (Stadtherr et al., 2016).

The datasets and methodology used for this study are provided in section 2. Section 3 focuses on the results; the section is subdivided to present a brief climatology of precipitation

84 and extreme precipitation events in the Northeastern United States, a composite analysis of
85 extreme precipitation events, an analysis of the impact of tropical cyclones and closed low
86 pressure systems on extreme precipitation events, and an indication of how the character of
87 extreme events has changed over time. A summary and discussion is provided in section 4.

88 **2. Data and Methods**

89 The primary tools for the analysis include observational and reanalysis products.
90 Observations of precipitation are from the Climate Prediction Center (CPC)'s gridded Unified
91 Gauge-Based Analysis of daily precipitation at a resolution of 0.25° by 0.25° (Xie et al. 2007;
92 Chen and Xie, 2008). The Modern-Era Retrospective Analysis for Research and Applications,
93 Version 2 (MERRA-2) was used to represent the large-scale circulation and meteorological
94 quantities that are not easily observed (Bosilovich et al. 2015; Gelaro et al. 2016, in prep).
95 Hourly data from MERRA-2 are available at a spatial resolution of 0.625° longitude by 0.5°
96 latitude, and daily averages ending at 12z were computed to match the temporal resolution of the
97 precipitation observations. MERRA-2 features additional observing systems and improvements
98 to the hydrological cycle not present in the original MERRA atmospheric reanalysis (Rienecker
99 et al. 2011), including the forcing of the land surface with observations-based precipitation fields
100 and the implementation of a moisture constraint, preventing an imbalance in global precipitation
101 and surface evaporation (Reichle and Liu, 2014; Takacs et al., 2016). MERRA-2 also features
102 numerous developments in the underlying model (Molod et al. 2015), such as in the surface layer
103 and boundary layer parameterizations and in the cumulus convection scheme. The data
104 assimilation has been updated to the latest Gridpoint Statistical Interpolation version and
105 includes global dry mass constraints that help minimize spurious temporal variability effects
106 (Takacs et al., 2016). Also, new observations not available to the original MERRA have been

added, such as GPS radio occultation and the Infrared Atmospheric Sounding Interferometer (McCarty et al., 2016).

We focus in this paper on the northeastern United States region outlined in Figure 1, a region that includes land areas between 40 and 45°N and 70 and 76°W. This region was selected based on an analysis of the seasonal climatological means and interannual variability over the past 30 years in an effort to reduce spatial variability in precipitation within the northeast region as defined by the National Climate Assessment (Horton et al., 2014). Figures that were used to further define the Northeast region can be seen in the supplemental document.

Using the CPC gauge observations, daily precipitation values for the area as a whole are computed, and percentiles are then calculated from these spatial averages among the days with at least 1 mm of precipitation, following Rivera et al. (2014), Hirata et al. (2015), and Westby et al. (2015). The 1 mm threshold is used to ensure that only days with a precipitation event are included in the percentile calculation. Keep in mind that the nature of our results will depend in part on the area used here for the averaging; larger regions may favor widespread heavy precipitation as opposed to local or regional extreme precipitation. Given the area we use, many of the events we examine are widespread and on the synoptic scale, impacting most of the region.

Percentiles were defined separately for each day of the year using a window around each date of ±1 week and then considering together the daily precipitation values during the 2-week period in each year from 1981 through 2010. This window around each date allows for more robust statistics while maintaining any differences associated with seasonality. Warm and cold season extreme precipitation events differ in frequency and intensity, and this methodology allows for seasonal variations in precipitation to be taken into account (Frei et al., 2015). In this

study, we focus on June, July, and August.

Frei et al. (2015) classified extreme precipitation events using 90th, 95th, and 99th percentiles, and the Climate Data Operators (CDO) and the Expert Team on Climate Change Detection and Indices (ETCCDI; Alexander et al., 2006) classified them using 75th, 95th and 99th percentiles. Here we focus on the 75th and 95th percentiles, with events falling into the category if they are within a range of ±5 percentile units of the noted values. That is, the 75th percentile grouping, or composite, does not include the more extreme events found in the 95th percentile composite and can thus be considered a composite of relatively weaker events. By definition, there are a similar number of events in both groupings (~200; see Table S1). This number is representative of roughly 10% of the number of days with at least 1 mm of precipitation as opposed to the total number of days within the time period due to the threshold used in the percentile calculation. Note that such a compositing approach has been used to study events (e.g., atmospheric rivers) in other regions (Grotjahn and Faure, 2008; Warner et al., 2012; Gao et al., 2014).

While MERRA-2 shows significant improvements over MERRA in the representation of extreme precipitation events, there are still uncertainties associated with modeled precipitation (Bosilovich et al., 2015). MERRA-2 and the CPC gauge data do not contain exactly the same number of days above 1 mm to be included in the percentile calculations and therefore do not result in the same number of events that exceed a given percentile. More importantly, there are a number of dates that are considered extreme in the observations and not in MERRA-2, and vice versa. As a result, only the observations are used here to determine whether an event falls in the 75th or 95th percentile categories. Using observations to determine extreme precipitation events and reanalysis data for the large-scale circulation is a common methodology used in past studies

153 (eg. Gao et al., 2014).

154 **3. Results**

155 *a. Climatology of the Northeastern United States*

156 Having both mountains and a coastline, the climate in the Northeast is greatly influenced
157 by geography, and the region is susceptible to different varieties of weather including hurricanes,
158 extratropical cyclones, mesoscale systems, heat waves, and drought during the summer months.
159 Mean climate features during JJA over the period of 1980 through 2014 in MERRA-2 are shown
160 in Figure 1. Temperature at 2 m tends to decrease with increasing latitude (Figure 1a). Cooler
161 temperatures over the ocean inhibit daytime warming along the coast and higher elevations
162 associated with the Appalachian Mountains result in cooler temperatures, most notably over
163 eastern New York. The mountains also play a role in mean daily precipitation, with precipitation
164 enhanced over the higher elevation (Figure 1b).

165 The availability of moisture is a key component of precipitation events, and information
166 about this availability, e.g. in the form of vertically integrated water vapor flux, is a unique
167 feature of reanalyses such as MERRA-2. Tropospheric winds are generally from the west, with
168 maximum velocities centered around 45 °N (Figures S1 and S2), resulting in a mean eastward
169 transport of water vapor (Figure 1c). Vertically integrated moisture fluxes positioned over land
170 are also higher near the coast, most notably over Rhode Island and Cape Cod, Massachusetts,
171 with the Atlantic Ocean serving as a source of moisture. Moisture from the Atlantic Ocean can
172 also be seen in the total precipitable water vapor (TPW) along the coast (Figure 1d).

173 While summertime extreme precipitation frequency has changed over time in numerous
174 locations within the United States, the Northeast shows the largest increase in the frequency of

extreme events at the 95th percentile, according to the CPC Gauge observations (Figure 2). The 95th percentile used for Figure 2 was defined for each 0.25° by 0.25° grid box in the observations. Most of the region has seen an increase greater than one such event per decade (Figure 2a). The significance of the trend was evaluated using a Monte Carlo simulation; results show that in many parts of the Northeast, the observed trend is significantly different from zero at the 99% confidence level (Figure 2b).

A time series for area-averaged observed precipitation within the region of interest is presented in Figure 3a (black curve). Based on a least squares regression and a Student-t test, there is a statistically significant upward trend in mean precipitation over the 36-year time period. A closer look at the time series indicates that the increase overtime is in fact superimposed on an oscillation or a shift that occurs in the late 1990s; this might be related to the Atlantic Multidecadal Oscillation, which has been shown to be positively correlated to summertime precipitation and extreme precipitation in the Northeast United States (Enfield et al., 2001; Curtis, 2008). It has been shown that the positive phase of the Atlantic Multidecadal Oscillation leads to an area of decreased sea level pressure and a cyclonic circulation off the east coast (Knight et al., 2006; Curtis, 2008). This cyclonic circulation is believed to increase the flow of low level moisture into the region that is forced to rise due orographic lift from the Appalachian Mountains, therefore leading to more frequent intense precipitation events.

While mean precipitation in the Northeast has increased over time, the median has not (Figure 3a, red curve). This implies that while extreme precipitation events are increasing, non-extreme events are not. This point is further emphasized in Figure 3b, which shows the time series of 75th and 95th percentile precipitation events (in terms of number of events). While there is considerable interannual variability in the number of 75th percentile precipitation events, their

198 frequency does not change over time. For the 95th percentile events, however, there is a steady
199 increase in number after the late 1990s, with a linear trend over the entire period that is
200 statistically significant at the 95% confidence interval.

201 *b. Composited Fields during Extreme Precipitation Events*

202 Using extreme precipitation events over the Northeast (as determined from the daily
203 gauge observations) as the basis for compositing, we compute composites of various
204 meteorological fields from MERRA-2. Total precipitation composited using the 75th and 95th
205 percentile Northeast precipitation events is shown in Figure 4. For both intensities, a wide area,
206 spanning the entire east coast, sees significant precipitation (on average) during these events. Our
207 methodology clearly pulls out large-scale events that cover an area much larger than the defined
208 Northeast region. The daily average precipitation may in fact capture precipitation from a system
209 that traveled through and impacted a different region earlier in the day. The composite based on
210 the 95th percentile indicates that the heaviest observed precipitation fell in the southern portion of
211 the Northeast region, along the coastline.

212 A key component of extreme precipitation events is the availability of moisture in the
213 region. Figure 5 shows the anomalous flow of moisture, more specifically, anomalies in the
214 vertically integrated water vapor flux, into the Northeast before, during, and after these events, as
215 represented by the two sets of composites. Values below 40 kg m^{-1} s^{-1} have been masked out to
216 draw attention to larger anomalies. From two days out there is little difference between
217 climatology and 75th percentile precipitation events, with the only anomaly being a hint of a
218 trough beginning to take shape in the Northern Great Plains and Midwest (Figure 5a). This
219 anomaly is amplified in magnitude and area in the 95th percentile composite, with the center
220 shifted to the south (Figure 5b). The day prior to an extreme precipitation event, the vertically

integrated moisture flux anomalies become stronger, forming a cyclonic circulation; again, the cyclonic circulation is stronger and slightly farther south in the 95th percentile anomaly composite (compare Figure 5c and d). Moisture flux anomalies are strongest in the southern portion of the circulation. Anomalies are likely stronger to the south from the convergence of moisture coming from the west and moisture from the Gulf of Mexico. The increased flow of moisture from the Atlantic Ocean apparent in the 95th percentile composite for the day prior to the event is somewhat deceptive. In that region, moisture fluxes in the composite are oriented from the southwest but are smaller than what is seen in the climatology, and this is manifested in the anomaly field as a change in direction that makes it look as if moisture is brought into the region from the Atlantic Ocean (Figure S3).

On the day of the extreme precipitation event, the circulation pattern represented by the vertically integrated moisture flux anomalies takes on an elongated shape, with a tilt from the southwest to northeast (Figures 5e and f). The largest anomalies are now on the east side of the circulation, with moisture being pulled in from the Atlantic Ocean in the warm conveyor belt of enhanced southerly flow. Anomalies extend further south in the 95th percentile events, with decreased moisture transport into Texas and Louisiana (Figure S3), and with an increased westerly and southwesterly flow of moisture in the southeastern portion of the country. The Gulf of Mexico serves as a moisture source for the 95th percentile composite but not so much for the 75th percentile composite. An additional difference between the 75th and 95th percentile events is seen in the easterly anomalies over the Atlantic Ocean, which are absent during 75th percentile events.

The day after the extreme precipitation event, the circulation pattern leaves the region with a shift toward the northeast. For the 75th percentile composite, as the pattern nears the

Atlantic Ocean, the region of maximum moisture flux anomalies is broader than it was on the day of the event.

As moisture is conveyed from the Gulf of Mexico and Atlantic Ocean, positive anomalies of total precipitable water vapor (TPW) develop over the Northeast, as seen in Figure 6. TPW anomalies are weak two days prior to an extreme precipitation event but become more significant the day before the event. Maximum TPW anomalies are centered east of the Great Lakes in both the 75^{th} and 95^{th} percentile cases; however, the anomalies are stronger for the latter composite. The shape of the 75^{th} percentile positive TPW anomaly is indicative of an extratropical cyclone, whereas the 95^{th} percentile anomaly appears broader. Relatively drier air develops to the west, concurrent with the enhanced northerly flow. TPW anomalies are stronger on the day of the event and become tilted from southwest to northeast, similar to what was seen with the vertically integrated moisture flux anomalies. As the system exits the region the following day, the magnitude of the anomaly does not decrease as the anomaly propagates eastward and moisture becomes available from the Atlantic Ocean.

The anomalies of the vertically integrated water vapor flux provide some indication of the overall flow in the troposphere during extreme precipitation events. However, wind anomalies in the upper troposphere, in this case at 250 hPa, can also provide information regarding the dynamics surrounding extreme precipitation events. This is illustrated in Figure 7. Anomalies below 3 m s^{-1} have been masked out to highlight the more significant anomalies. In the climatology (not shown), the strongest winds in the jet stream are located between 40 and 50 °N with a general westerly flow. Two days prior to an extreme precipitation event, a stronger meridional component of the 250 hPa winds is seen along the US-Canada border around Montana and the Great Lakes. On the day before the event, these wind anomalies become

267 stronger and develop a cyclonic pattern centered around Minnesota. Wind speed divergence is
268 seen in the Midwest region, with directional divergence to the northeast along the border of
269 Ontario and Quebec. This divergence in the upper troposphere can signal convergence at the
270 surface and upward vertical motion in the column, a suitable component to an extreme
271 precipitation event.

272 The strongest 250 hPa wind anomalies are present on the day of the extreme precipitation
273 event, with maxima in the northwest quadrant of the selected Northeast region. The entire region
274 is located in the right entrance region of enhanced upper level winds, where upward vertical
275 motion occurs. These maxima in the anomaly fields are oriented toward the northeast in the 75th
276 percentile events but have a more northward orientation in the 95th percentile events.

277 Two days prior to an extreme precipitation event, a trough develops upstream of the
278 region of interest in both the 75th and 95th percentile composites of 500 hPa heights (Figure 8a
279 and b). The negative height anomaly is generally stronger and located slightly to the south in the
280 95th percentile case. In both cases the trough is embedded in a wave train oriented east to west.
281 The trough tracks to the southeast with movement slowing between the day of and the day after
282 an extreme precipitation event.

283 Notice in Figure 8 that the low-high dipoles around the event are stronger in magnitude
284 for the 95th percentile composite. The negative anomaly in 500 hPa height is accompanied by a
285 similar pattern in sea level pressure anomalies, though the low pressure system is not vertically
286 stacked (Figure 9). The positive anomaly to the east of the negative anomaly at 500 hPa develops
287 coherently with the low in sea level pressure in the 95th percentile composite, but not in the 75th.
288 Negative sea level pressure anomalies become elongated the day of the event and the day after
289 the event. The shape of the negative sea level pressure anomaly, particularly in the 95th percentile

290 case the day after the event, resembles a low pressure system and trailing cold front.

291 A reduction in cut off lows has been shown to be responsible for a reduction in
292 precipitation in southern Australia, and a change in blocking patterns could cause the opposite
293 response in the United States (Risbey et al., 2013). Following the methodology of Pook et al.
294 (2006), an event was determined to be caused by a cut off low if MERRA-2 indicated a closed
295 area of sea level pressure below 1008 hPa with a trough at 500 hPa, or a closed contour in 500
296 hPa height, alongside a negative anomaly in 1000 hPa to 500 hPa thickness of at least 20 m
297 compared to climatology within the synoptic region. The number of 95th percentile extreme
298 precipitation events related to cut off lows as a function of year is shown in Figure 10a, along
299 with the time series of the total number of extreme events. While there is a statistically
300 significant increasing trend in events caused by a cut off low, this trend is not large enough to
301 account for the total observed increase in extreme precipitation events in the Northeast. On the
302 other hand, despite year-to-year variability, there is no change over time in the number of 75th
303 percentile events caused by cut off lows.

304 *d. Tropical Extreme Precipitation Events*

305 Previous studies of extreme precipitation events in the Northeast indicate that the
306 percentage of summertime extreme events caused by tropical cyclones can exceed 25% (Kunkel
307 et al., 2012; Agel et al., 2015). This number is very dependent on the methodology used to define
308 an extreme event and a tropical cyclone. Following Kunkel et al. (2012), we define an extreme
309 Northeast event to be caused by a tropical cyclone if a storm listed in the National Hurricane
310 Center's North Atlantic hurricane database (HURDAT) was within 5° of the Northeast region.
311 Given our definition of an extreme event as falling within plus or minus 5 percentile units of the
312 95th percentile, we find the percentage of extreme precipitation events in JJA caused by a tropical

313 cyclone to be a relatively low 10.6%, though we are focusing on a smaller region than in the
314 previous studies and are using percentile based approach to define events. In contrast, Kunkel et
315 al. (2012) use a threshold (which does not vary with time of year) to define events based on a
316 return period of five years, and they areal average the number of events caused by tropical
317 cyclones for a larger spatial area, one that spans Maine through West Virginia.

318 Most of the extreme events we have linked to tropical cyclones are in the more recent
319 time period; only two occur in the 1980s (Figure 11a), and both of these events are related to
320 tropical storm Chris, which traveled through the region in 1988 as a tropical depression. There is
321 no significant linear trend in the time series of events caused by tropical cyclones during 1985-
322 2014, as there are never more than two events in a given year. The total number of extreme
323 precipitation events per year, on the other hand, does have a statistically significant trend (Figure
324 3b).

325 The average intensity of an event is somewhat determined by the methodology used to
326 define an event, and this intensity hovers around 20 mm day^{-1} for all events (Figure 11b). Aside
327 from 2011 and 2013, which saw nearly doubled intensities due to Hurricane Irene and Tropical
328 Storm Andrea, the average intensity of the tropical cyclone-related events is roughly the same.
329 The total seasonal precipitation from extreme events (Figure 11c) is thus more closely related to
330 the number of events than their intensity. There are a number of years without any hurricanes but
331 with a high total accumulation from extreme events (e.g., 1982, 1998, and 2006). While the
332 largest accumulation from extreme events occurred in 2011, coinciding with the maximum
333 average intensity due to tropical cyclones, overall there is no statistically significant indication
334 that tropical cyclones are responsible for the increase in extreme precipitation events in the
335 Northeast.

When events caused by a tropical cyclone are removed from the 95th percentile events, the composited sea level pressure and 500 hPa heights on the day of the extreme precipitation events (not shown) do not change much from those seen in Figures 8f and 9f. This is likely due to the fact that only a small fraction of events were removed – only 21 out of ~200 95th percentile precipitation events between 1980 and 2014 matched a tropical cyclone in HURDAT. Figure 12 shows the sea level pressures composited on these 21 cyclone-related events. (Note that there were not enough events in the 75th percentile category to allow a corresponding analysis.) Leading up to the day of an extreme precipitation event, an area of suppressed sea level pressure can be seen coming up the coast rather than moving in from the northwest, as in Figure 9 (for all 95th percentile events). There is a wider trough in sea level pressure for the tropical cyclone-related events, though caution must be taken with a direct comparison due to the fact that the different composites are based on a different number of events. One commonality between Figures 9 and 12 is the region of a positive sea level pressure anomaly to the northeast, helping to steer the region of low pressure.

e. Change in Composites Over Time

To examine factors that may induce changes in extreme precipitation over time, we compare composites from the first half of the MERRA-2 time period (1980 though 1996) to those constructed from the second half (1997 through 2014) using the same time series of extreme events as the previous composites. Time difference composites (later period minus early period) for sea level pressure, 500 hPa heights, vertically integrated moisture fluxes, precipitation, Eady growth rate, and a vertical cross section of equivalent potential temperature on the day of a 95th percentile precipitation event are shown in Figure 13. Note that in contrast to the previous figures, which showed anomalies relative to climatology, Figure 13 shows the

359 difference in the total fields between the two time periods. Most of the United States saw a
360 decrease in sea level pressure, though the only region with a statistically significant decrease
361 extends from Maine through northeastern Florida (Figure 13a). The shape of this statistically
362 significant region is reminiscent of a cold front with the northern edge over the eastern half of
363 the selected region, but this can also be indicative of cut off lows or extratropical cyclones. Cold
364 fronts are a significant contributor to summertime extreme precipitation events in the Northeast
365 (Kunkel et al., 2012) and are a potential factor towards the observed increase in extreme
366 precipitation events.

367 A region of reduced 500 hPa height during 95th percentile events is also present in the
368 later period (Figure 13b). It was shown earlier that events are not vertically stacked, and this is
369 also indicated by the time difference plots. The region of decreased 500 hPa height lies to the
370 west of the region of decreased sea level pressure, and it also lies to the south, perhaps indicating
371 that more events are taking a track more analogous to a nor'easter rather than an Alberta clipper.
372 An area of statistically significant higher heights is located to the northeast, showing an increase
373 in the pressure gradient over time during extreme precipitation events. Moisture fluxes have also
374 strengthened, particularly over the Gulf Stream (Figure 13c).

375 In agreement with the trends seen in Figure 2, the time differenced composite of observed
376 precipitation during 95th percentile events shows an increase through the eastern portion of New
377 York (Figure 13d). On the other hand, Connecticut, Rhode Island, and Massachusetts have
378 experienced a decrease in this extreme precipitation. Apparently, during the second half of the
379 evaluated time period, the events identified as extreme according to the area-averaged
380 precipitation tended to occur farther to the west, increasing the precipitation in New York and
381 decreasing the precipitation near the coast. This is somewhat in agreement with Figure 2, which

382 does not show a significant trend in extreme precipitation events in Massachusetts, Connecticut,
383 or Rhode Island.

384 Baroclinic instability can be a measure of the potential for "storminess" within a region,
385 and one metric for this is the Eady growth rate (Hoskins and Valdes, 1990). The change in the
386 maximum Eady growth rate, computed for the layer of 700 to 300 hPa, between 1980 though
387 1996 and 1997 through 2014 during 95th percentile precipitation events is shown in Figure 13e.
388 The northern edge of the region overlaps a strip of decreased Eady growth rate over time, while
389 there is an increase to the south. This may indicate a southward shift in storm tracks.
390 Extratropical cyclones are typically located further north in the summer compared to the winter;
391 a southerly shift in Eady growth rate in the summer, however, would indicate that the region
392 could experience more events related to extratropical systems. The statistically significant
393 increase in Eady growth rate just south of the region would place an extratropical cyclone in an
394 ideal location for an onshore flow of moisture into the region along with the dynamics required
395 for precipitation to develop. A comparison to future projections of Eady mean growth rate can be
396 seen in the supplemental material.

397 In order to determine if there is a thermodynamic component to the observed changes
398 related to extreme precipitation events, a cross section of the vertical profile of equivalent
399 potential temperature, θ_e, and specific humidity at 42 N was analyzed. A constant latitude was
400 chosen through the center of the region. An increase in θ_e, as indicated by red shading in Figure
401 13f, and specific humidity, indicated by solid black contours, over time can be seen at the surface
402 over the region. These increases slant eastward with increasing height and extend through 300
403 hPa for θ_e ; however, humidity is confined to a shallower region within the troposphere. Cooler
404 and drier air lags behind, aside from the increase in θ_e in the upper troposphere. The eastward

405 slant with height in thermodynamic properties furthers the suggestion of an increase in extreme
406 precipitation events associated with frontal activity, though additional work is needed to fully
407 determine if the frequency or intensity of frontal systems have changed over time.

408 **4. Summary and Discussion**

409 Extreme precipitation events can have large impacts on society, and observations indicate
410 that these events have increased during the months of June, July, and August in the Northeastern
411 United States. This increase in extreme precipitation events is statistically significant and is the
412 largest and most widespread change in extreme precipitation in the United States. Based on
413 future climate projections, it is possible this trend will continue, sparking the need for a greater
414 understanding of the details surrounding extreme precipitation events in the Northeast (IPCC,
415 2013; Janssen et al., 2014).

416 In this paper, we examine in detail the character of meteorological fields associated with
417 extreme precipitation events in the Northeast. With observational precipitation records, we
418 construct composites from MERRA-2 of general circulation and synoptic structure leading up to,
419 during, and following extreme precipitation events. Overall, the composites provide evidence of
420 extratropical cyclones that pass through the Northeastern United States and produce large
421 amounts of rainfall, with stronger anomalies in dynamical quantities seen for the 95^{th} percentile
422 events. Lower pressures at the surface and divergence aloft allow for upward vertical motion,
423 while the flow around the low pressure area and the high pressure to the east from the associated
424 wave train conveys moisture into the region sufficient enough for heavy rainfall.

425 Previous studies show the summer time atmospheric circulation has weakened, with an
426 increase greater than 40% in high amplitude days in 500 hPa height contours during July,

August, and September (Francis and Vavrus, 2015; Francis and Skific 2015) and an increase in JJA North Atlantic blocking events (Barnes et al, 2014; Hanna et al., 2015; Hanna et al., 2016). As a result, in combination with the trend in Eady growth rate, baroclinic systems that produce extreme events are becoming more stationary. With the Atlantic Ocean providing a vast moisture supply, and with the increasing occurrence of quasi-stationary low pressure systems and frontal systems, extreme precipitation events in the Northeast have become more common. These dynamics have also been demonstrated in studies looking at blocking high pressure systems in relation to Arctic Amplification (Coumou et al., 2015). Dynamical changes in addition to the "wet gets wetter" theory and the ability of warmer air to hold more moisture are likely contributors to the increase in extreme precipitation.

Note that convective events are not well represented in our composites. In this paper we identify extreme events by considering precipitation averaged over the Northeast area outlined in Figure 1, and this area is substantially larger than the spatial scale of individual convective events. In effect, our analysis focuses by construction on large-scale events and the associated character of the large-scale circulation. In addition, by using daily averages of meteorological fields, we further average out characteristics of events that are not caused by large-scale, synoptic features.

There is, of course, still much we can learn about extreme precipitation events in the Northeast using these techniques. There are indications, for example, that extreme events stemming from frontal systems should be separated in our compositing analysis from those associated with extratropical cyclones, given that fronts are a leading cause of summertime extreme precipitation events (Kunkel et al., 2012; Catto and Pfahl, 2013), in order to further explore the nature of frontal systems and their connection to the changing extreme precipitation.

Also, while our composites show little change when tropical cyclones are removed, this does not necessarily mean that tropical cyclones are not contributing to the increase in extreme precipitation events; it only says that a small percentage of summertime events are caused by tropical cyclones. Using reanalysis data to composite extreme events with a full classification of the underlying systems that generate the extreme rainfall should provide useful information.

Acknowledgments

This work was supported by NASA's Earth Science Research Program. CPC US Unified Precipitation data was provided by the NOAA/OAR/ESRL PSD, Boulder, Colorado, USA, from their website at http://www.esrl.noaa.gov/psd/. MERRA-2 data was developed by the Global Modeling and Assimilation Office at NASA GSFC and disseminated through the Goddard Earth Science Data Information Services Center (GES DISC). HURDAT was provided by NOAA/HRD.

5. References

Agel, L., M. Barlow, J. H. Qian, F. Colby, E. Douglas, and T. Eichler, 2015: Climatology of daily precipitation and extreme precipitation events in the Northeast United States, *Journal of Hydrometeorology*, **16**, 2537-2557, doi: *http://dx.doi.org/10.1175/JHM-D-14-0147.1*.

Alexander, L. V., and Coauthors, 2006: Global observed changes in daily climate extremes of temperature and precipitation. *J. Geophys. Res*., **111**, D05109, doi: 10.1029/2005JD006290.

Barlow, M., 2011: Influence of hurricane-related activity on North American extreme precipitation*, Geophys. Res. Lett*., **38**, L04705, doi:10.1029/2010GL046258.

472 Barnes, E. A., E. Dunn-Sigouin, G. Masato and T. Woollings, 2014: Exploring recent trends in
473 Northern Hemisphere blocking. *Geophysical Research Letters*, **41**,
474 doi: 10.1002/2013GL058745.

475 Bosilovich, M. G., et al., 2015: MERRA-2: Initial evaluation of the climate, *Technical Report*
476 *Series on Global Modeling and Data Assimilation*, **43**, NASA/TM-2015-104606.

477 Catto, J. L., C. Jakob, G. Berry, and N. Nicholls, 2012: Relating global precipitation to
478 atmospheric fronts, *Geophys. Res. Lett*., **39**, L10805, doi:10.1029/2012GL051736.

479 Catto, J. L., and S. Pfahl, 2013: The importance of fronts for extreme precipitation, *J. Geophys.*
480 *Res. Atmos*., **118**, 10,791–10,801, doi:10.1002/jgrd.50852.

481 Chen, M., and P. Xie, 2008: CPC Unified Gauge-based Analysis of Global Daily Precipitation,
482 Western Pacific Geophysics Meeting, 29 July – 1 August 2008, Cairns, Australia.

483 Coumou, D., J. Lehmann, and J. Beckmann, 2015: The weakening summer circulation in the
484 Northern Hemisphere mid-latitudes. *Science*, **348**, 324-327, doi:
485 10.1126/science.1261768.

486 Curtis, S., 2008: The Atlantic multidecadal oscillation and extreme daily precipitation over the
487 US and Mexico during the hurricane season. *Clim. Dyn.,* **30**, 343-351, doi:
488 10.1007/s00382-007-0295-0.

489 Enfield, D.B., A.M. Mestas-Nuñez, and P.J. Trimble, 2001: The Atlantic Multidecadal
490 oscillation and its relation to rainfall and river flows in the continental US. *Geophysical*
491 *Research Letters*, **28**, 2077-2080, doi: 10.1029/2000GL012745.

492 Francis, J. A. and S. J. Vavrus, 2015: Evidence for a wavier jet stream in response to rapid Arctic
493 warming. *Environmental Research Letters*, **10**, doi:10.1088/1748-9326/10/1/014005.

494 Francis, J.A. and N. Skific, 2015: Evidence linking rapid Arctic warming to mid-latitude weather
495 patterns. *Phil. Trans. R. Soc*. A, **373**, doi:10.1098/rsta.2014.0170.

496 Frei, A. K. E. Kunkel, and A. Matonse, 2015: The seasonal nature of extreme hydrological
497 events in the Northeastern United States. *J. Hydrometeor*, **16**, 2065–2085, doi:
498 http://dx.doi.org/10.1175/JHM-D-14-0237.1.

499 Gao, X., C. A. Schlosser, P. Xie, E. Monier, and D. Entekhabi, 2014: An analogue approach to
500 identify heavy precipitation events: Evaluation and application to CMIP5 climate models
501 in the United States. *J. Clim*, **27**, 5941–5963, doi: http://dx.doi.org/10.1175/JCLI-D-13-
502 00598.1.

503 Gelaro, R. and co-authors, 2016: The MERRA-2 Project. In Preparation for *J. Clim*.

504 Grotjahn, R. and G. Faure, 2008: Composite predictor maps of extraordinary weather events in
505 the Sacramento, California, Region*. *Weather and Forecasting*, **23**, 313-335, doi:
506 http://dx.doi.org/10.1175/2007WAF2006055.1.

507 Hanna, E., T. E. Cropper, P. D. Jones, A. A. Scaife, and R. Allan, 2015: Recent seasonal
508 asymmetric changes in the NAO (a marked summer decline and increased winter
509 variability) and associated changes in the AO and Greenland Blocking Index. *Int. J.*
510 *Climatol*, **35**, 2540–2554. doi:10.1002/joc.4157.

511 Hanna, E., T. E. Cropper, R. J. Hall, and J. Cappelen, 2016: Greenland Blocking Index 1851–
512 2015: a regional climate change signal. *Int. J. Climatol*., in press, doi:10.1002/joc.4673.

513 Horton, R., G. Yohe, W. Easterling, R. Kates, M. Ruth, E. Sussman, A. Whelchel, D. Wolfe, and
514 F. Lipschultz, 2014: Ch. 16: Northeast. Climate change impacts in the United States: The
515 Third National Climate Assessment, J. M. Melillo, Terese (T.C.) Richmond, and G. W.

516 Yohe, Eds., *U.S. Global Change Research Program*, 16-1-nn.

517 Hirata, F. E. and A. M. Grimm, 2015: The role of synoptic and intraseasonal anomalies in the
518 life cycle of summer rainfall extremes over South America. *Climate Dynamics*, in press,
519 doi: 10.1007/s00382-015-2751-6.

520 Hoskins, B. J. and P. J. Valdes, 1990: On the existence of storm-tracks. *J. Atoms. Science*, **47**,
521 1854-1864, doi: 10.1175/1520-0469(1990)047<1854:OTEOST>2.0CO;2.

522 IPCC, 2013: Summary for Policymakers. In: Climate Change 2013: The Physical Science Basis.
523 Contribution of Working Group I to the Fifth Assessment Report of the
524 Intergovernmental Panel on Climate Change [Stocker, T.F., D. Qin, G.-K. Plattner, M.
525 Tignor, S.K. Allen, J. Boschung, A. Nauels, Y. Xia, V. Bex and P.M. Midgley (eds.)].
526 Cambridge University Press, Cambridge, United Kingdom and New York, NY, USA.

527 Ivancic, T. J., and S. B. Shaw, 2016: A US-based analysis of the ability of the Clausius-
528 Clapeyron relationship to explain changes in extreme rainfall with changing
529 temperature. *J. Geophys. Res. Atmos*., **121**, 3066-3078, doi: 10.1002/2015JD024288.

530 Janssen, E., D. J. Wuebbles, K. E. Kunkel, S. C. Olsen, and A. Goodman, 2014: Observational-
531 and model-based trends and projections of extreme precipitation over the contiguous
532 United States, *Earth's Future*, **2**, doi:10.1002/2013EF000185.

533 Knight, J. R., C. K. Folland, and A. A. Scaife, 2006: Climate impacts of the Atlantic
534 Multidecadal Oscillation, *Geophys. Res. Lett*., **33**, L17706, doi:10.1029/2006GL026242.

535 Konrad II, C. E., 2001: The Most Extreme Precipitation Events over the Eastern United States
536 from 1950 to 1996: Considerations of Scale. *J. Hydrometeor*, **2**, 309–325, doi:
537 10.1175/1525-7541(2001)002<0309:TMEPEO>2.0.CO;2.

538 Kunkel, K. E., D. R. Easterling, D. A. R. Kristovich, B. Gleason, L.Stoecker, and R. Smith,
539 2012: Meteorological causes of the secular variations in observed extreme precipitation
540 events for the Conterminous United States. *J. Hydrometeor*, **13**, 1131–1141, doi:
541 http://dx.doi.org/10.1175/JHM-D-11-0108.1.

542 Kunkel, K. E. and Coauthors, 2013: Regional climate trends and scenarios for the U.S. National
543 Climate Assessment: Part 1. Climate of the Northeast U.S. NOAA Tech. Rep. NESDIS
544 142-1, 80pp.

545 McCarty, W., and co-authors, 2016: MERRA-2 Input Observations: Summary and Initial
546 Assessment, *Technical Report Series on Global Modeling and Data Assimilation*, **45**,
547 NASA/TM-2016-104606, in preparation.

548 Melillo, J. M., T. C. Richmond, and G. W. Yohe, 2014: Ch. 2: Our Changing Climate. *Climate*
549 *Change Impacts in the United States: The Third National Climate Assessment*, U.S.
550 Global Change Research Program, 19-67. doi:10.7930/J0KW5CXT.

551 Molod, A., L. Takacs, M. Suarez, M., J. and Bacmeister, 2015: Development of the GEOS-5
552 atmospheric general circulation model: evolution from MERRA to MERRA2, *Geosci.*
553 *Model Dev*., **8**, 1339-1356, doi:10.5194/gmd-8-1339-2015.

554 Pook, M. J., P. C. McIntosh, and G. A. Meyers, 2006: The Synoptic Decomposition of Cool-
555 Season Rainfall in the Southeastern Australian Cropping Region, *Journal of Applied*
556 *Meteorology and Climatology*, **45**, 1156-1170, doi: 10.1175/JAM2394.1.

557 Reichle, R. H., and Q. Liu, 2014: Observation-corrected precipitation estimates in GEOS-5.
558 *NASA/TM–2014-104606*, Vol. **35.**

559 Rienecker, M. M., and Co-Authors, 2011: MERRA, NASA's Modern-Era Retrospective

560 Analysis for Research and Applications. *J. Climate*, **24**, 3624-3648, doi:
561 http://dx.doi.org/10.1175/JCLI-D-11-00015.1.

562 Risbey, J. S., P. C. McIntosh, and M. J. Pook, 2013: Synoptic components of rainfall variability
563 and trends in southeast Australia. *Int. J. Climatol*., **33**, 2459–2472, doi:10.1002/joc.3597.

564 Rivera, E. R., F. Dominguez, and C. L. Castro, 2014: Atmospheric rivers and cool season
565 extreme precipitation events in the Verde River Basin of Arizona. *J. Hydrometeor*, **15**,
566 813–829, doi: http://dx.doi.org/10.1175/JHM-D-12-0189.1.

567 Stadtherr, L., D. Coumou, V. Petoukhov, S. Petri, and S. Rahmstorf, 2016: Record Balkan floods
568 of 2014 linked to planetary wave resonance. *Science Advances*, **2**, e1501428, doi:
569 10.1126/sciadv.1501428.

570 Takacs, L.L., M.J. Suárez, and R. Todling, 2016: Maintaining atmospheric mass and water
571 balance in reanalyses. *Quart. J. Roy. Meteor. Soc.*, accepted, doi: 10.1002/qj.2763.

572 Warner, M. D., C. F. Mass, and E. P. Salathé Jr., 2012: Wintertime extreme precipitation events
573 along the Pacific Northwest coast: Climatology and synoptic evolution. *Mon. Wea. Rev*.,
574 **140**, 2021–2043, doi: http://dx.doi.org/10.1175/MWR-D-11-00197.1.

575 Westby, R. M., R. X. Black, 2015: Development of anomalous temperature regimes over the
576 Southeastern United States: Synoptic behavior and role of low-frequency modes.
577 *Weather and* Forecasting, **30**, 553-570, doi: http://dx.doi.org/10.1175/WAF-D-14-
578 00093.1.

579 Xie, P., A. Yatagai, M. Chen, T. Hayasaka, Y. Fukushima, C. Liu, and S. Yang, 2007: A gauge-
580 based analysis of daily precipitation over East Asia, *J. Hydrometeorol*., **8**, 607-626, doi:
581 http://dx.doi.org/10.1175/JHM583.1.

582

6. Figure Captions

Figure 1: Mean June, July, and August (a) 2 m temperature, (b) precipitation, (c) vertically integrated water vapor fluxes, and (d) total precipitable water vapor over the period of 1980 through 2014. The Northeast region as defined in this study is outlined in black.

Figure 2: (a) Trend in the number of June, July, and August precipitation events at the 95th percentile (b) Significance of the trend in (a) as calculated using a Monte Carlo simulation.

Figure 3: (a) Area averaged mean and median observed precipitation in the Northeast United States during June, July, and August from 1979 through 2014, (b) The number of 75th and 95th percentile precipitation events in the Northeast United States during June, July, and August. Trends calculated with a least squares progression are given in parentheses and asterisks indicate statistical significance at a 95% confidence interval.

Figure 4: Observed precipitation composited during (a) 75^{th} percentile events and (b) 95^{th} percentile events.

Figure 5: Vertically integrated water vapor flux anomalies composited from two days prior to one day after an observed 75th (left column) and 95th (right column) percentile precipitation event. Anomalies below 40 kg m^{-1} s^{-1} are masked out.

Figure 6: Total precipitable water vapor anomalies composited from two days prior to one day after an observed 75th (left column) and 95th (right column) percentile precipitation event. Hatching denotes regions with a statistical significance of 95%.

Figure 7: 250 hPa wind anomalies composited from two days prior to one day after an observed 75th (left column) and 95th (right column) percentile precipitation event. Anomalies below

604 3 m s^{-1} are masked out.

605 Figure 8: 500 hPa height anomalies composited from two days prior to one day after an observed
606 75th (left column) and 95th (right column) percentile precipitation event. Hatching denotes
607 regions with a statistical significance of 95%.

608 Figure 9: Sea level pressure anomalies composited from two days prior to one day after an
609 observed 75th (left column) and 95th (right column) percentile precipitation event. Hatching
610 denotes regions with a statistical significance of 95%.

611 Figure 10: Time series of the number of total events and those caused by a cut off low for the (a)
612 95^{th} percentile and (b) 75^{th} percentile.

613 Figure 11: (a) Time series of number of total and tropical 95^{th} percentile events in the Northeast
614 during June, July, and August. (b) Time series of the average intensity of a 95^{th} percentile event
615 in the Northeast during June, July, and August. (c) Time series of the total amount of
616 precipitation from a 95^{th} percentile event for all events and those caused by a tropical cyclone in
617 the Northeast during June, July, and August.

618 Figure 12: Sea level pressure anomalies composited from two days prior to one day after a 95th
619 percentile precipitation event caused by a tropical cyclone. Hatching denotes regions with a
620 statistical significance of 95%.

621 Figure 13: The difference in (a) sea level pressure, (b) 500 hPa height, (c) vertically integrated
622 moisture flux, (d) observed precipitation, (e) Eady growth rate, and (f) the vertical profile of
623 equivalent potential temperature at 42 N composites during 95^{th} percentile precipitation events
624 calculated by subtracting the mean composite for 1980 through 1996 from the composite for
625 1997 through 2014. Hatching denotes regions with a statistical significance of 95%.

626 **Figures**

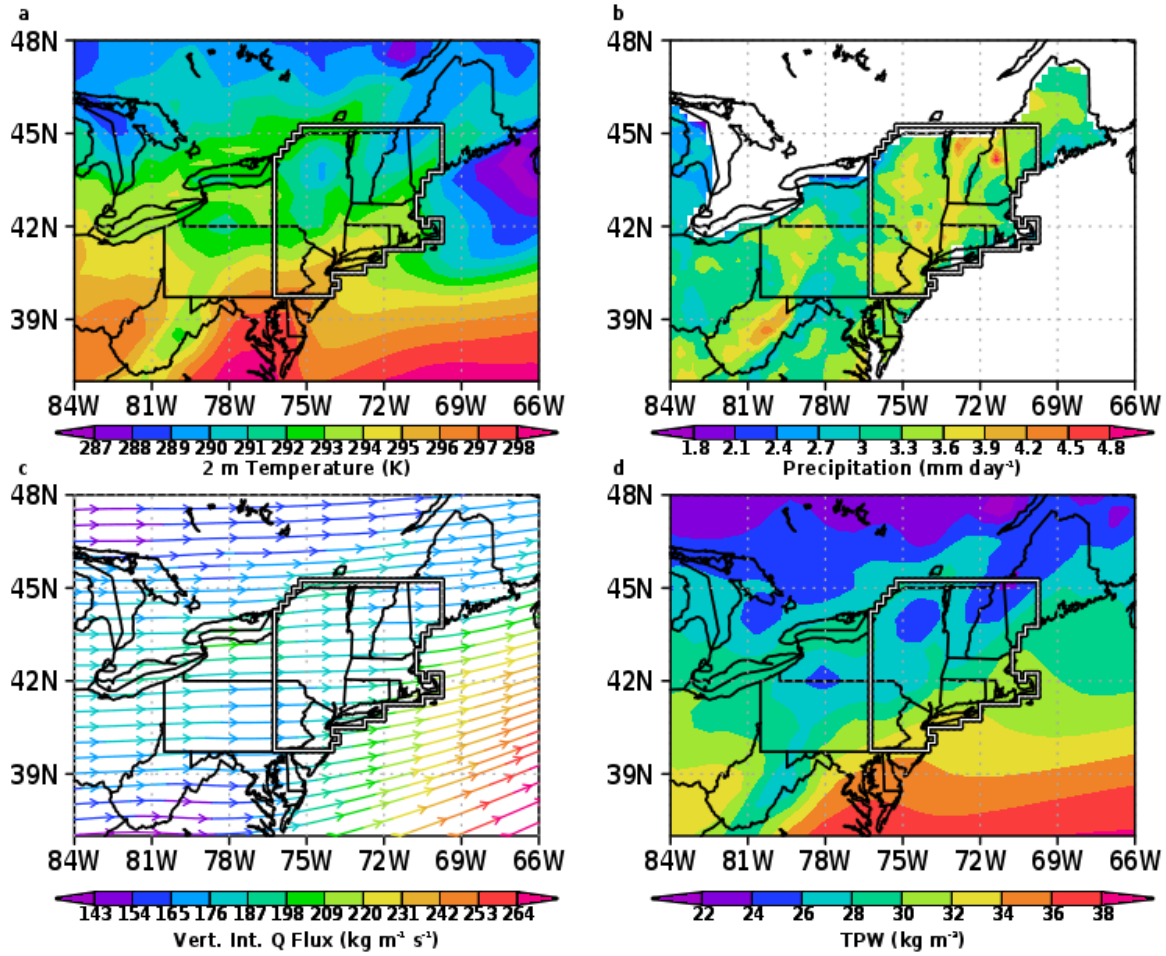

627

628 Figure 1: Mean June, July, and August (a) 2 m temperature, (b) precipitation, (c) vertically
629 integrated water vapor fluxes, and (d) total precipitable water vapor over the period of 1980
630 through 2014. The Northeast region as defined in this study is outlined in black.

631

632

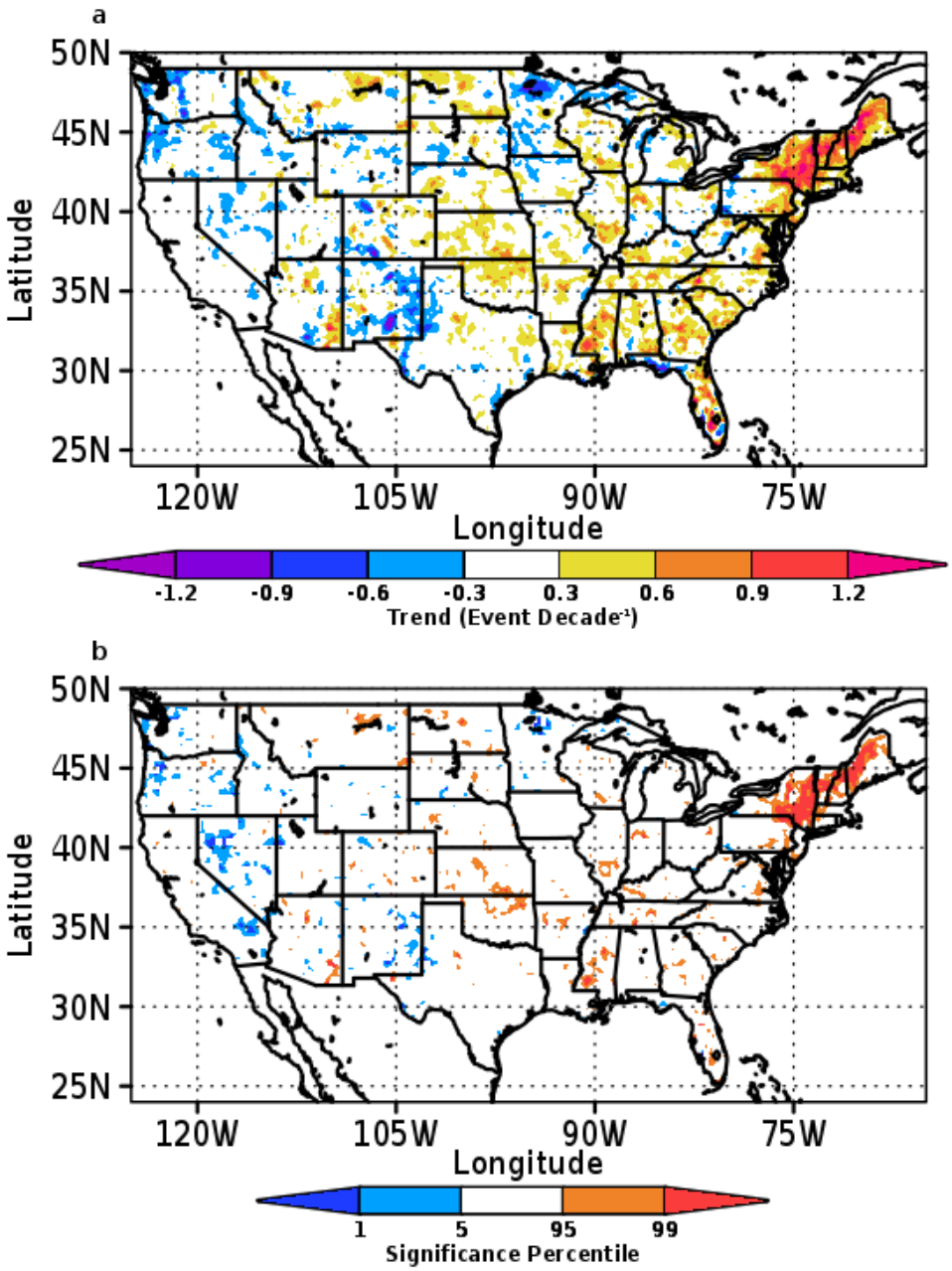

633

634 Figure 2: (a) Trend in the number of June, July, and August precipitation events at the 95th
635 percentile (b) Significance of the trend in (a) as calculated using a Monte Carlo simulation.

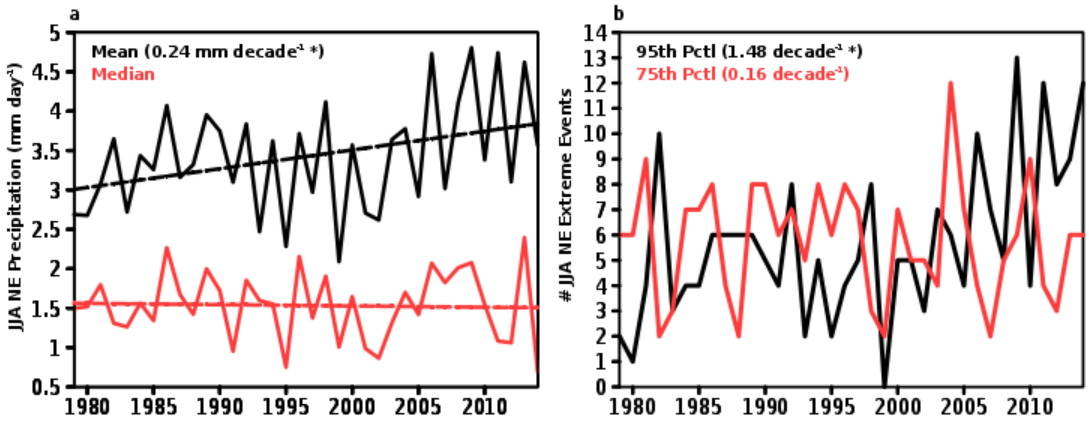

636

637 Figure 3: (a) Area averaged mean and median observed precipitation in the Northeast United
638 States during June, July, and August from 1979 through 2014, (b) The number of 75th and 95th
639 percentile precipitation events in the Northeast United States during June, July, and August.
640 Trends calculated with a least squares progression are given in parentheses and asterisks indicate
641 statistical significance at a 95% confidence interval.

642

643

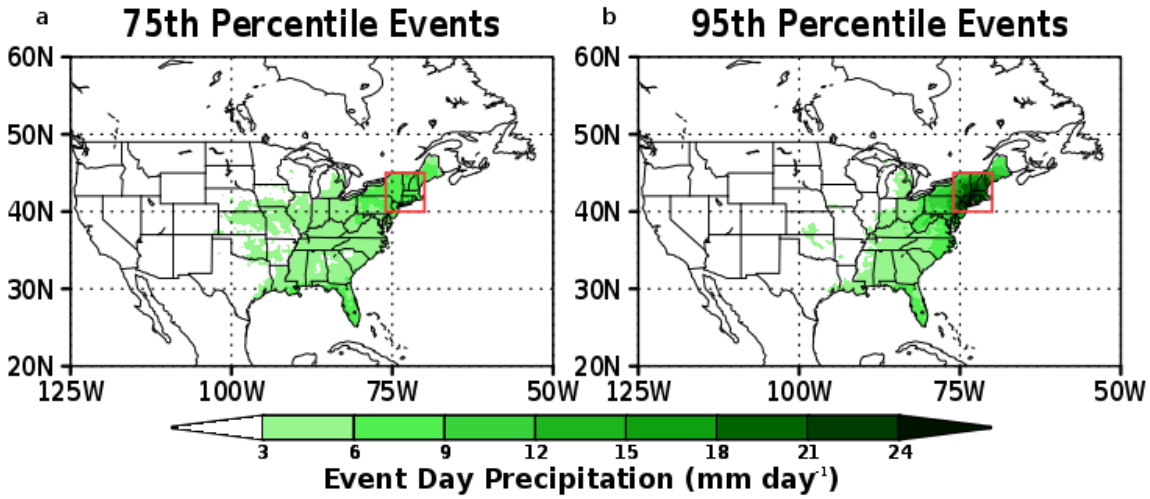

644

645 Figure 4: Observed precipitation composited during (a) 75th percentile events and (b) 95th

646 percentile events.

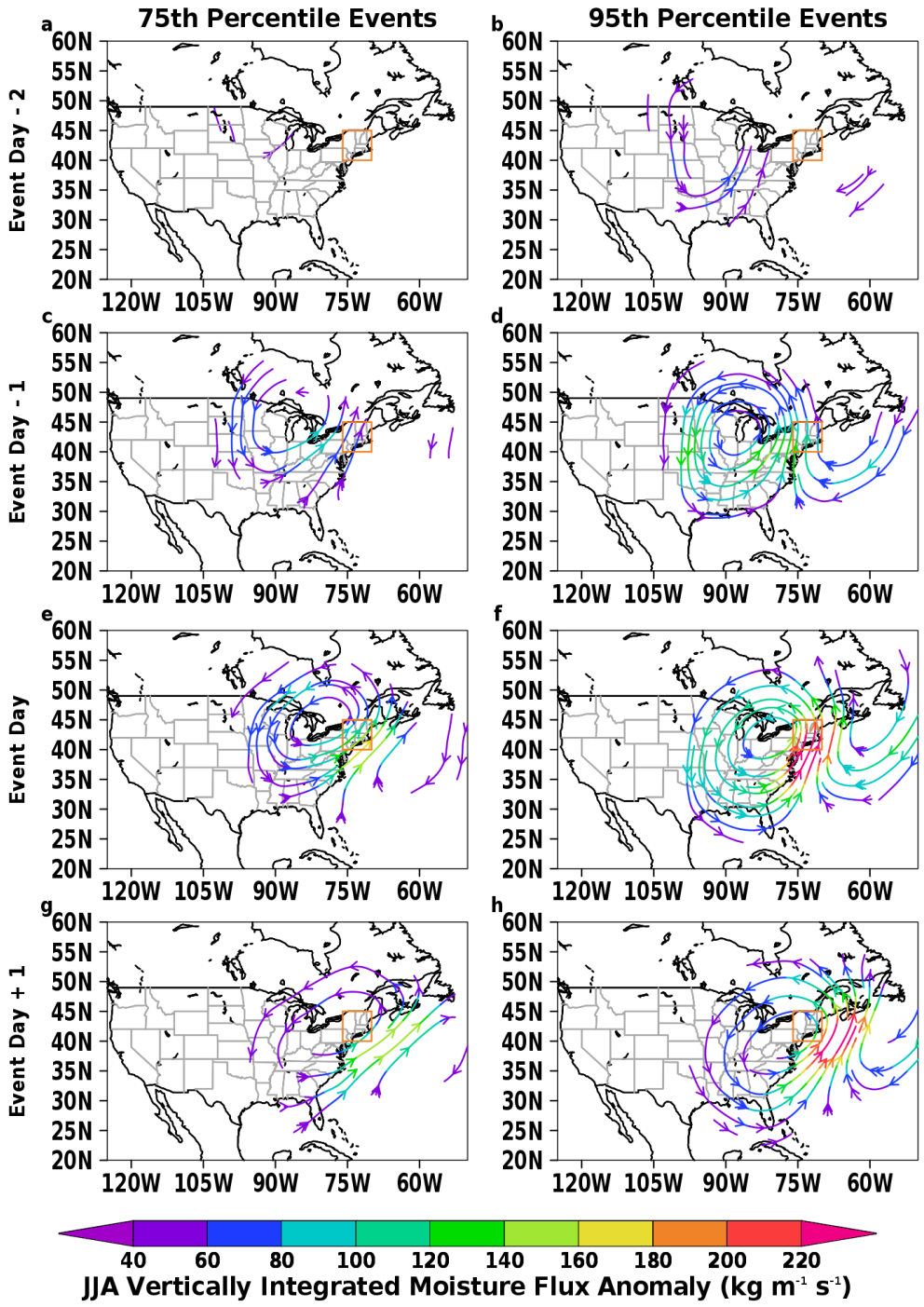

Figure 5: Vertically integrated water vapor flux anomalies composited from two days prior to one day after an observed 75th (left column) and 95th (right column) percentile precipitation event. Anomalies below 40 kg m^{-1} s^{-1} are masked out.

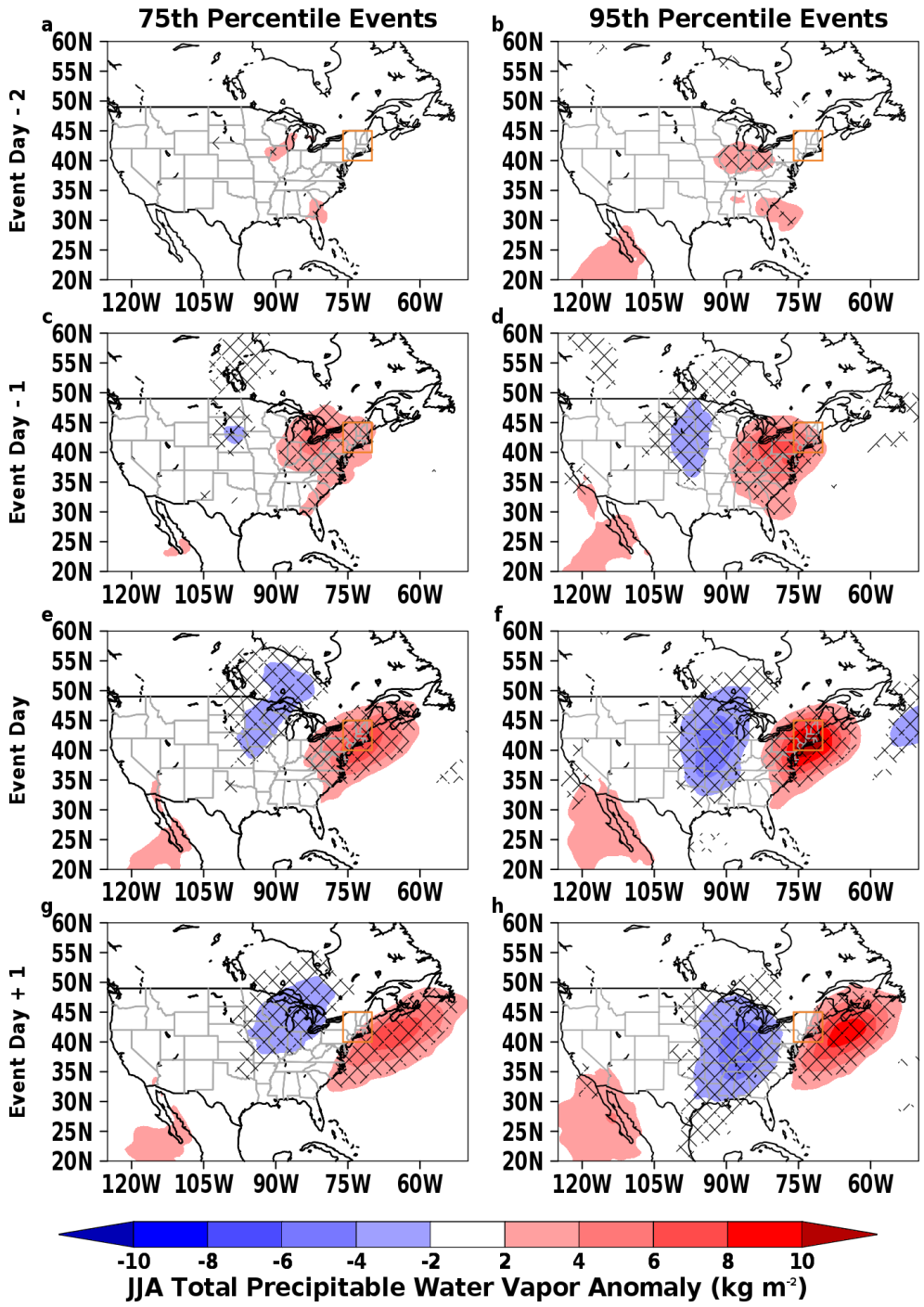

651

652 Figure 6: Total precipitable water vapor anomalies composited from two days prior to one day
653 after an observed 75th (left column) and 95th (right column) percentile precipitation event.
654 Hatching denotes regions with a statistical significance of 95%.

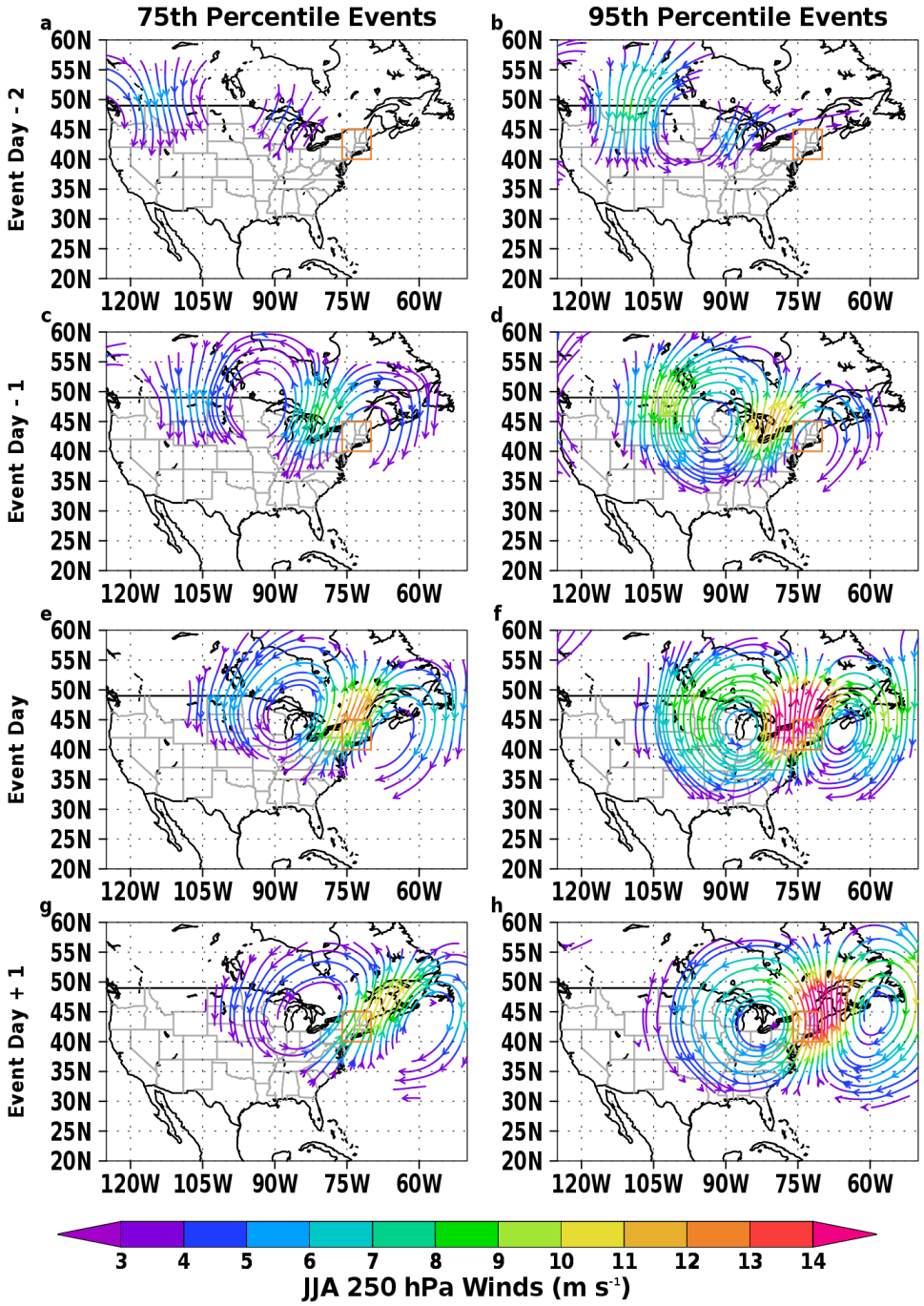

Figure 7: 250 hPa wind anomalies composited from two days prior to one day after an observed 75th (left column) and 95th (right column) percentile precipitation event. Anomalies below 3 m s^{-1} are masked out.

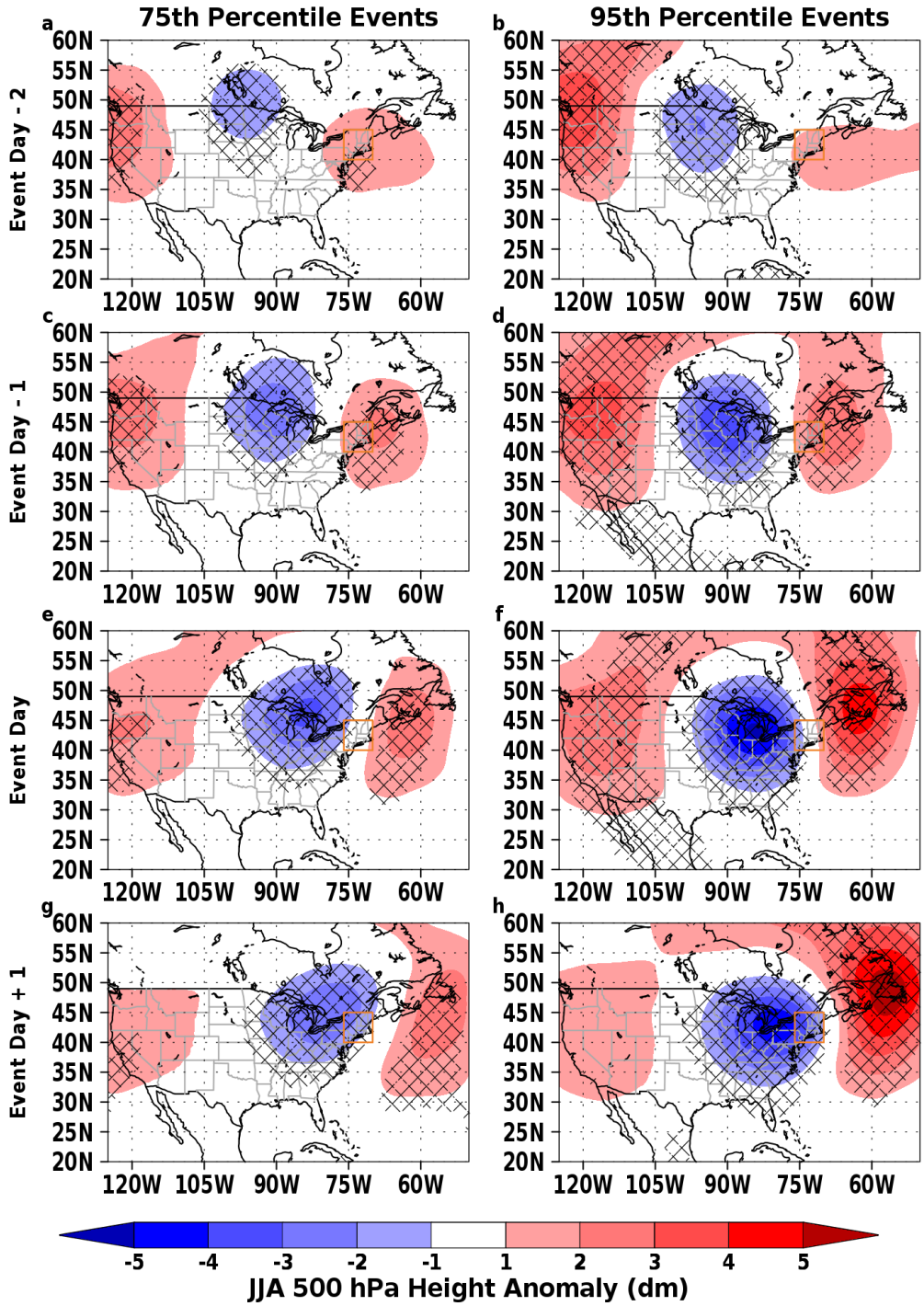

Figure 8: 500 hPa height anomalies composited from two days prior to one day after an observed 75th (left column) and 95th (right column) percentile precipitation event. Hatching denotes regions with a statistical significance of 95%.

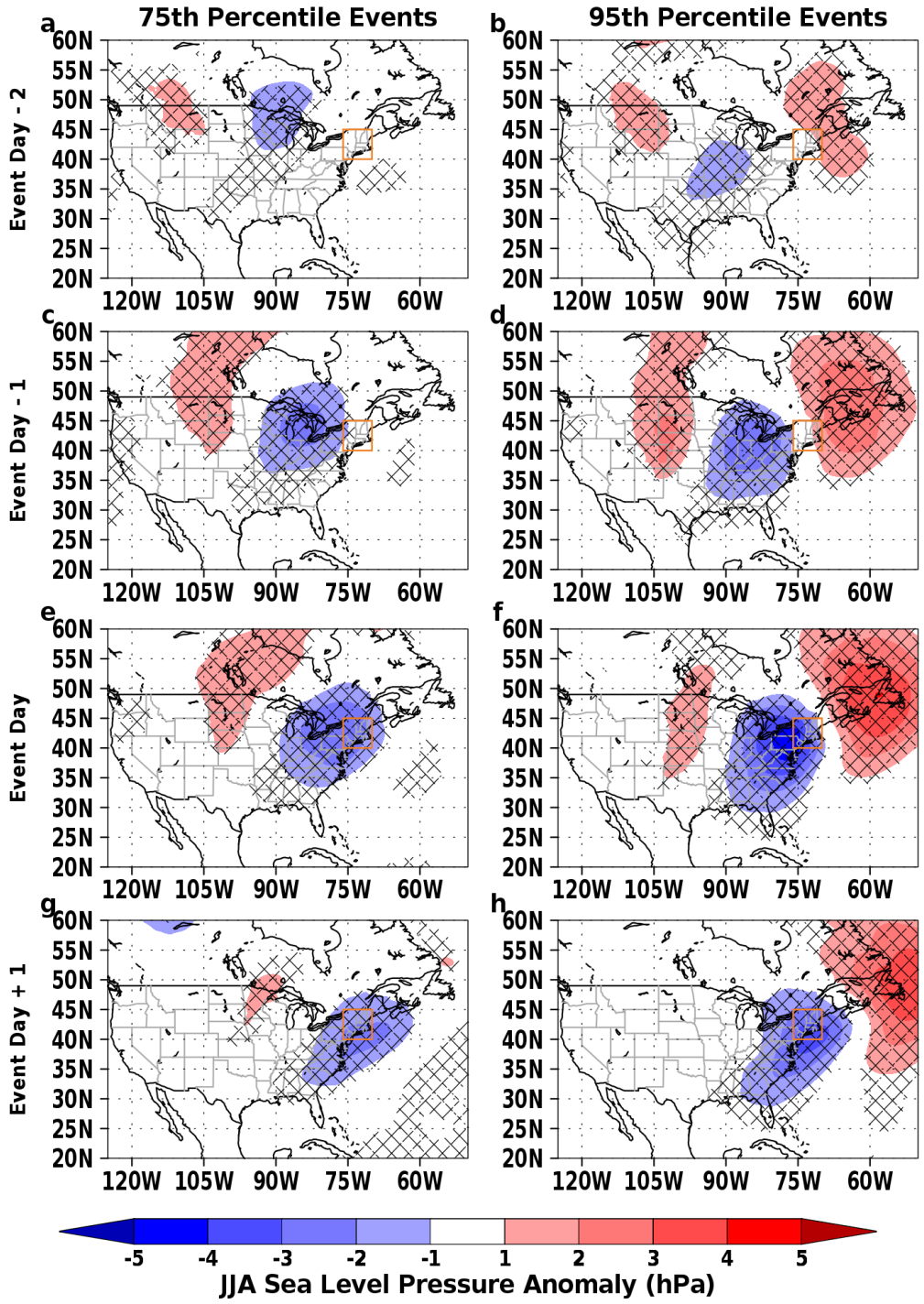

Figure 9: Sea level pressure anomalies composited from two days prior to one day after an observed 75th (left column) and 95th (right column) percentile precipitation event. Hatching denotes regions with a statistical significance of 95%.

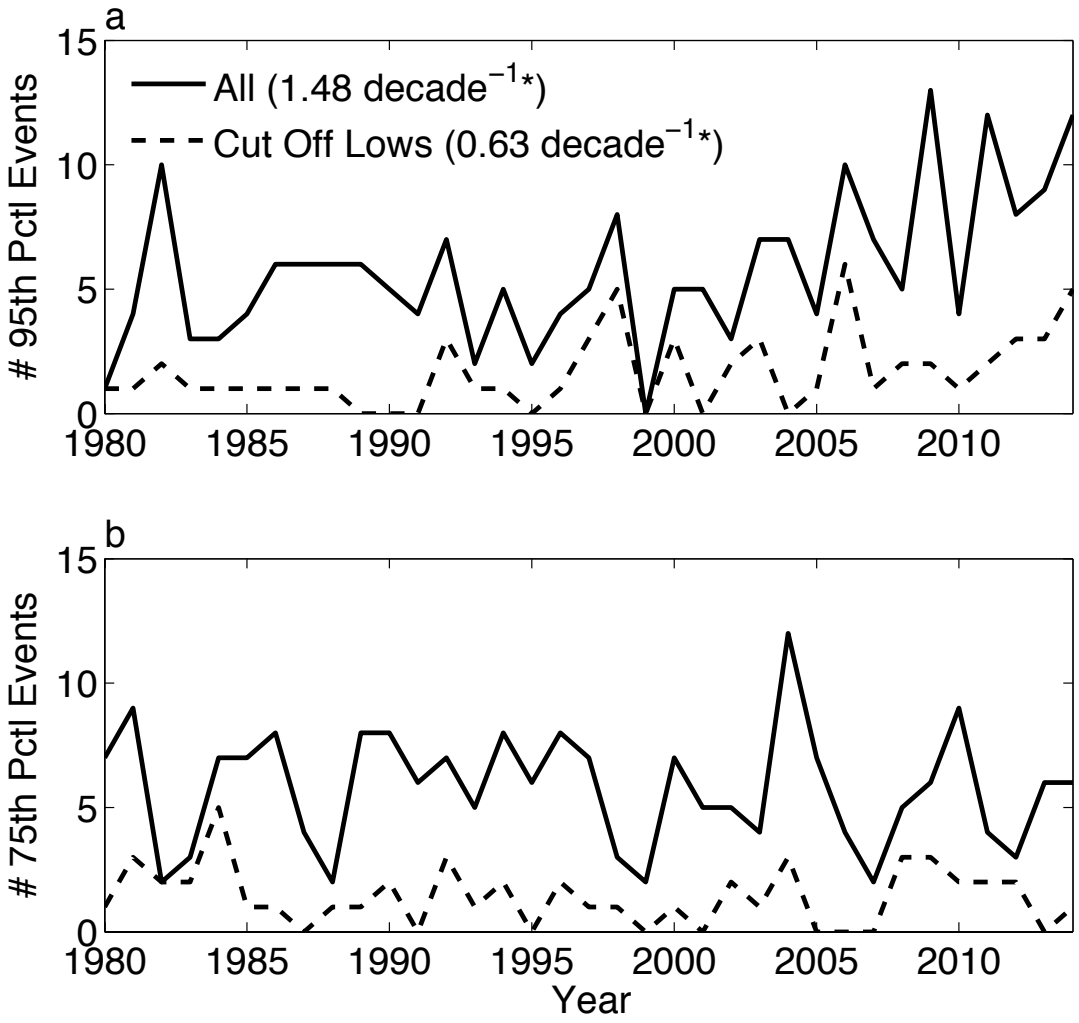

667

668 Figure 10: Time series of the total number of extreme events and the number caused by a cut off

669 low for the (a) 95th percentile and (b) 75th percentile.

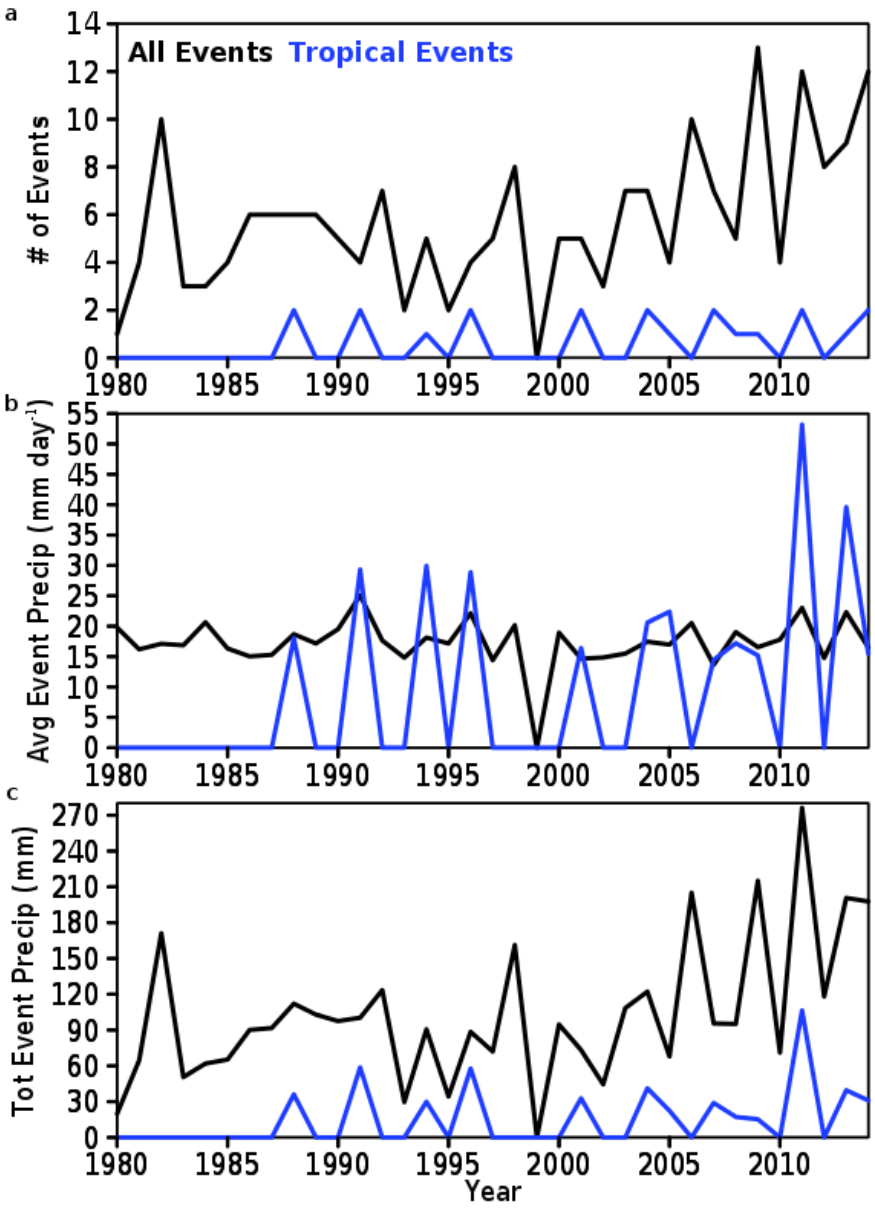

Figure 11: (a) Time series of number of total and tropical 95th percentile events in the Northeast during June, July, and August. (b) Time series of the average intensity of a 95th percentile event in the Northeast during June, July, and August. (c) Time series of the total amount of precipitation from a 95th percentile event for all events and those caused by a tropical cyclone in the Northeast during June, July, and August.

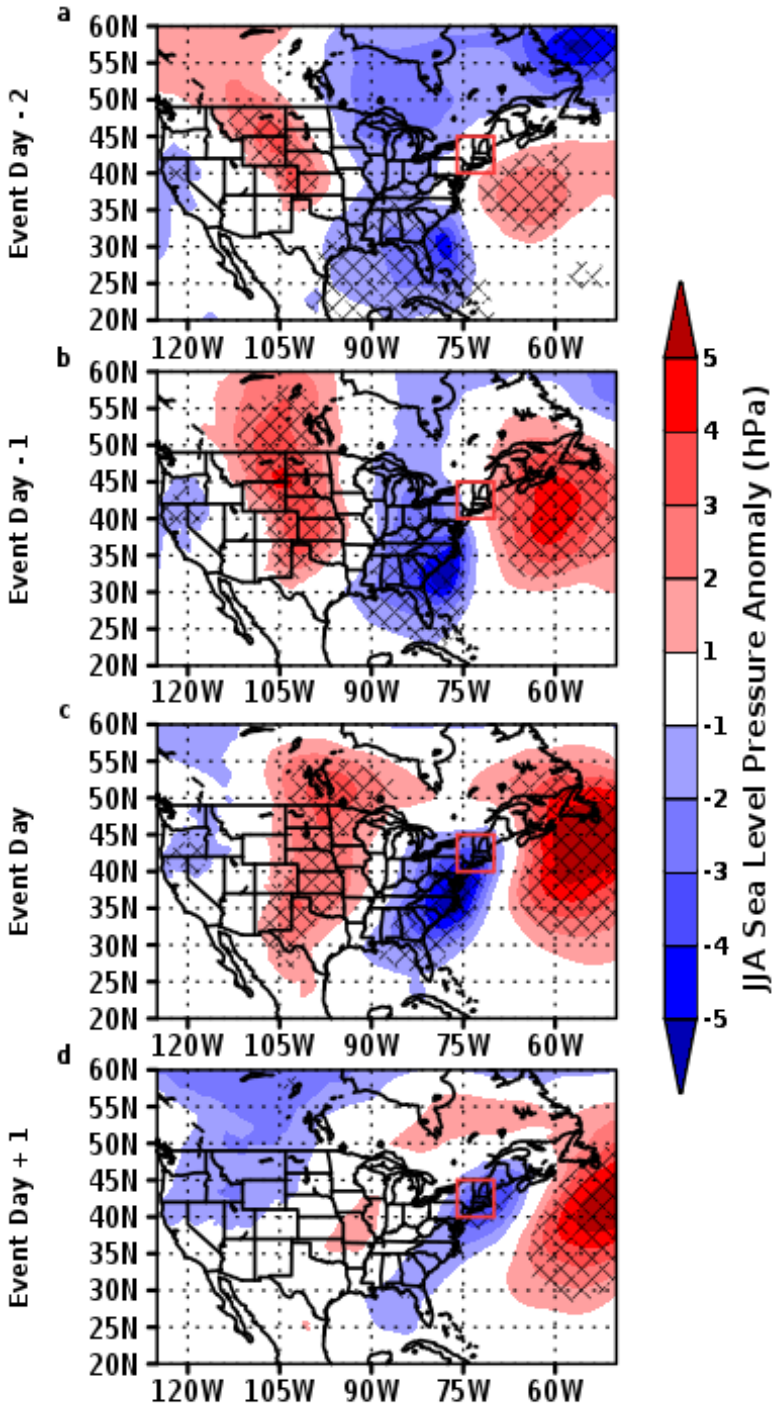

677

678 Figure 12: Sea level pressure anomalies composited from two days prior to one day after a 95th
679 percentile precipitation event caused by a tropical cyclone. Hatching denotes regions with a
680 statistical significance of 95%.

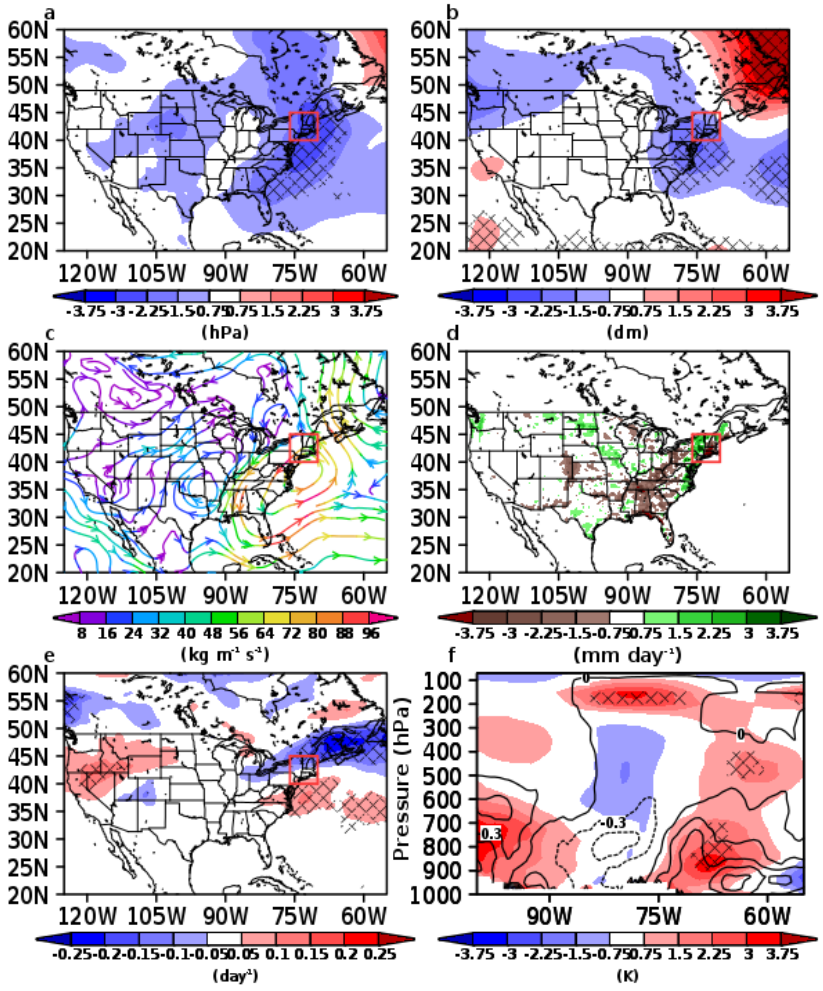

681

682 Figure 13: The difference in (a) sea level pressure, (b) 500 hPa height, (c) vertically integrated
683 moisture flux, (d) observed precipitation, (e) Eady growth rate, and (f) the vertical profile of
684 equivalent potential temperature at 42 N composites during 95th percentile precipitation events
685 calculated by subtracting the mean composite for 1980 through 1996 from the composite for
686 1997 through 2014. Hatching denotes regions with a statistical significance of 95%.

687